Vertical average for modeling seawater intrusion

M. Pool,[1,2] J. Carrera,[2] M. Dentz,[2] J. J. Hidalgo,[3] and E. Abarca[3]

Received 25 January 2011; revised 26 September 2011; accepted 30 September 2011; published 8 November 2011.

[1] Seawater intrusion in coastal aquifers is a 3-D phenomenon. However, 3-D regional aquifer models are often limited by insufficient geological and hydrological data, the large horizontal to vertical scales ratio, and by numerical constraints. We present an effective formulation for modeling seawater intrusion that relies on a dimensional reduction of the original density-dependent flow and transport problem. We carry out a vertical integration of the 3-D problem and arrive at a coupled set of 2-D equations for the mean flux and salt concentration, which are essentially identical to those of 2-D groundwater flow. However, two new terms emerge from the integration: (1) Darcy's law needs not only the buoyancy term reflecting aquifer bottom slope, but also another one reflecting variability of aquifer thickness; and (2) transport requires a new term reflecting vertical variations of groundwater flux, which are essential for density-dependent flow and we approximate by means of a Fickian dispersion term. The proposed equations are verified by direct steady state numerical simulations of confined aquifers. The results show that the effective formulation correctly reflects the effective dynamics in the 3-D system.

Citation: Pool, M., J. Carrera, M. Dentz, J. J. Hidalgo, and E. Abarca (2011), Vertical average for modeling seawater intrusion, *Water Resour. Res., 47*, W11506, doi:10.1029/2011WR010447.

1. Introduction

[2] Seawater intrusion in coastal aquifers is a three-dimensional phenomenon. Freshwater tends to float on top of seawater and a mixing zone develops between them. Seawater disperses across this mixing zone and is subsequently returned to the sea by freshwater discharge, thus forming a convection cell [*Cooper*, 1959]. The spatial distribution and temporal evolution of this convection cell are controlled by hydraulic properties, recharge, and pumping (Figure 1).

[3] The 3-D simulation of seawater intrusion is well documented [*Xue et al.*, 1995; *Oude Essink*, 2001a, 2001b; *Gingerich and Voss*, 2002; *Langevin*, 2003; *Qahman and Larabi*, 2006; *Lin et al.*, 2009]. However, 3-D modeling of regional coastal aquifers suffers from a large number of drawbacks [*Oude Essink and Boekelman*, 1996]. The horizontal extent of coastal aquifers is usually much greater than their thickness (different spatial scales), so that 3-D modeling usually requires an anisotropic spatial discretization, much larger in the horizontal than in the vertical direction, which enhances numerical dispersion and computational cost. Moreover, detailed 3-D geological and hydrological data are rarely available on a regional scale with the result that the undertaking may be in vain. In summary, it may not be reasonable to treat regional aquifers as 3-D entities. It is not surprising, therefore, that attempts have been made to simplify modeling of seawater intrusion.

[4] The most obvious simplification consists of working with equivalent freshwater head (elevation of a freshwater column yielding the observed pressure) while ignoring density differences. This approach neglects buoyancy forces within the domain, which may be appropriate when flow is largely controlled by viscous forces. This approach reproduces the seawater recirculation cell when driven by variations in the elevation of the aquifer-ocean boundary [*Sakr*, 1999; *Simpson and Clement*, 2003; *Dentz et al.*, 2006]. It may also be considered adequate in large aquifers, where flow is driven by inland boundary conditions or internal sink and sources [*Iribar et al.*, 1997; *Vazquez-Sune et al.*, 2006; *Abarca et al.*, 2006]. However, by neglecting buoyancy, this approach looses the most distinctive feature of seawater intrusion and its associated dynamics. Moreover, these models typically yield very sharp seawater intrusion patterns. That is, large portions of the model are fully salinized (salinity equal to that of seawater), whereas in reality most wells display (vertically averaged) salinities that are only a portion of seawater salinity.

[5] A higher level of sophistication is provided by sharp interface models in which freshwater and seawater are treated as two immiscible fluid phases [*Kacimov and Sherif*, 2006; *Bakker*, 1998, 2003; *Sa da Costa and Wilson*, 1979; *Ataie-Ashtiani*, 2007]. This simplification allows us to simulate seawater intrusion with 2- or 3-D models while acknowledging buoyancy. These models are appropriate whenever mixing can be neglected and they become particularly convenient under steady state conditions when seawater is not pumped, so that saltwater fluxes are small compared to freshwater ones, and saltwater head gradients

[1]Hydrogeology Group (GHS), Department of Geotechnical Engineering and Geosciences, Universitat Politecnica de Catalunya, UPC, Barcelona-Tech, Barcelona, Spain.
[2]GHS, Institute of Environmental Assessment and Water Research (IDAEA), Spanish Research Council (CSIC), Barcelona, Spain.
[3]Department of Civil and Environmental Engineering, Massachusetts Institute of Technology (MIT), Cambridge, United States.

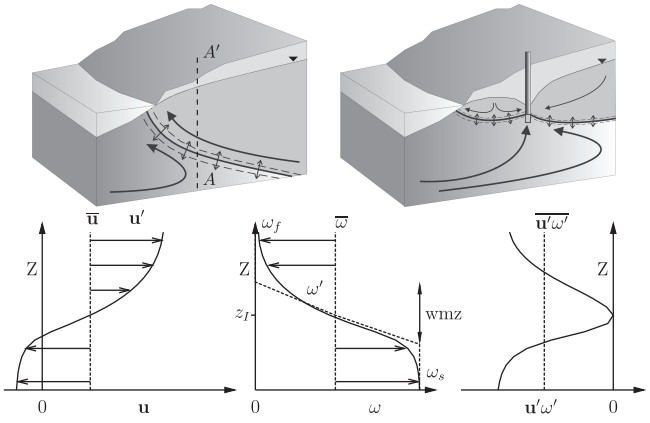

Figure 1. Vertical saltwater circulation cell, left, driven by buoyancy caused by mixing at the freshwater-seawater interface. Landward advance of the interface, right, induced by pumping. Seawater circulation no longer occurs on a vertical plane. Vertical variation of mass flux (**u**), salt mass fraction (ω), with ω_f and ω_s, the freshwater and seawater salt mass fraction, respectively, and the product of the fluctuations about their mean values ($\mathbf{u}'\omega'$) in the cross section A–A′ shown.

can be neglected. This together with the Dupuit assumption facilitates linearization and the derivation of analytical solutions [*Strack*, 1976], which has made the approach popular for the design of optimal pumping schemes [*Cheng et al.*, 2000; *Qahman et al.*, 2005; *Mantoglou*, 2003; *Mantoglou et al.*, 2004]. The sharp interface assumption is relaxed in boundary layer approximations and continues to assume seawater to be immobile but acknowledges salt transport across a narrow mixing zone [*Paster and Dagan*, 2007].

[6] The main disadvantage of the above approaches arises from neglecting mixing as a driving force for seawater flux. If mixing is sizeable, then seawater must flow inland to replenish the salt that is transported back to the sea by freshwater (Figure 1). The magnitude of mixing is controlled by transverse dispersion. Increasing transverse dispersion leads to an increase in the width of the mixing zone, to a landward seawater flux along the aquifer bottom, and hence to a retreat of the seawater intrusion wedge [*Abarca et al.*, 2007a]. Unfortunately, the role and magnitude of transverse dispersion have not yet been resolved. *Paster and Dagan* [2007], basing themselves on field observations, argue that transverse dispersion is negligible. On the other hand, *Abarca et al.* [2007a] reviewed a number of cases with sizeable mixing zones that required sizeable transverse dispersion. Moreover, heterogeneity and wind- or tide-induced sea level fluctuations enhance transverse dispersion [*Dentz and Carrera*, 2005, 2007]. Worse, even a small transverse dispersivity leads to a sizable effect on the location of the interface [*Pool and Carrera*, 2011].

[7] Our study was prompted by cases in which mixing plays a major role, for instance, regional coastal aquifers. In such cases, it is necessary to rely on fully coupled density-dependent flow and transport models, which require significant computation time.

[8] One common approach to circumvent the computational cost inherent in 3-D simulations consists in modeling a vertical 2-D cross-section [*Henry*, 1964; *Lahm et al.*, 1998; *Zhang et al.*, 2002; *Smith*, 2004; *Dentz et al.*, 2006; *Bolster et al.*, 2007]. Vertical 2-D cross-sections provide physical insight into the dynamics of seawater intrusion but not into realistic flow scenarios however simplified. This is the rationale for 2-D subhorizontal regional models. Certainly, the main component of flow in regional models is horizontal. Subhorizontal seawater convection cells are generated when the aquifer displays a lateral slope [*Abarca et al.*, 2007b]. It can therefore be assumed, that the vertical flow is of subleading order and can be neglected. This behavior may be reproduced by an areal 2-D model by averaging the 3-D flow and transport equations vertically. This has been studied by a number of authors assuming the sharp interface approximation [*Weiss*, 1982; *Maas and Emke*, 1988; *Sorek et al.*, 2001; *Bakker*, 2003; *Nordbotten and Celia*, 2006; *Gasda et al.*, 2009].

[9] Unfortunately, the above studies rarely address the potential divergence between freshwater and saltwater flux. As illustrated in the bottom of Figure 1, saltwater tends to flow inland along the aquifer bottom whereas freshwater floats on top as it flows seaward. Vertical integration involves working with averaged fluxes and concentrations. However, vertical fluxes induce mixing mechanisms that are lost in the simplified 2-D areal model, leading to differences in toe positions, width of the mixing zone, velocity distributions, and mass balance. One might conjecture that vertical integration should include the impact of the fluctuations about the spatial mean mass flux ($\mathbf{u}'$) and salt mass fraction (ω') in the governing equations in order to take into account the effect of this mechanism on dispersion. However, the effect of the mixing mechanism induced by vertical fluctuations in horizontal fluxes has not yet been studied.

[10] To illustrate the above, let us consider steady state conditions, where the mean salt flux is zero because all the salt that enters the aquifer along the bottom must exit along the mixing zone, to prevent accumulation of salt within the aquifer. Therefore, the total seaward water flux is equal to that of freshwater. Yet, average concentration is nonzero, so that integrated advection would carry salt seaward. This advective flux could only be offset by an inland dispersive flux. This dispersive flux must equal $\overline{\mathbf{u}'\omega'}$. We conjecture that it should be large because fluctuations about their mean values of both mass flux and salt mass fraction are

highly correlated (Figure 1) and that, consistently with stochastic transport results [e.g., *Gelhar and Axness*, 1983], it can be approximated by a Fickian dispersion term.

[11] Here a vertically integrated formulation is presented for modeling regional seawater intrusion. The objectives of this paper are (1) to test whether the conjecture of representing the inland salt flux by a dispersion term is valid, and (2) to ascertain whether this simplified formulation correctly reflects the effective dynamics in a fully dimensional system.

2. Governing Equations

2.1. Fully Dimensional Model

[12] The formulation presented in this paper is based on a vertical integration of the standard variable-density Darcy's law and the flow and transport equations [see, e.g., *Bear*, 1972]. The origin of coordinates is located at the coastline and the z-axis points vertically upward. Fluid density, ρ $[ML^{-3}]$, is assumed to be a linear function of the salt mass fraction ω $[M^3M^{-3}]$ (mass of dissolved salt per unit mass of fluid),

$$\rho = \rho_f \left(1 + \epsilon \frac{\omega}{\omega_s}\right), \tag{1}$$

where ω_s is the salt mass fraction in seawater; $\epsilon = (\rho_s - \rho_f)/\rho_f$ with ρ_f and ρ_s the freshwater and seawater densities, respectively (typical values of ϵ are $\sim$1/40).

[13] Momentum conservation in flow through porous media is expressed by Darcy's law, which we write in terms of equivalent freshwater head ($h = p/\rho_f g + z$) as

$$\mathbf{q} = -K \cdot \left[\nabla h + \epsilon \frac{\omega}{\omega_s} \widehat{e_g}\right], \tag{2}$$

where $\mathbf{q}$ is volumetric water flux $[LT^{-1}]$ and the freshwater conductivity $K[LT^{-1}]$ is assumed to be isotropic for simplicity. The unit vector $\widehat{e_g}$ points upward against gravity.

[14] The fluid mass balance in the absence of sources and sinks is given by

$$\frac{\partial(\rho\phi)}{\partial t} = \rho_f S_s \frac{\partial h}{\partial t} + \frac{\rho_f \epsilon}{\omega_s} \phi \frac{\partial \omega}{\partial t} = \nabla \times \mathbf{u}, \tag{3}$$

where $\mathbf{u}$ denotes mass flux ($\rho\mathbf{q}$), ϕ $[L^3L^{-3}]$ is porosity, and S_s $[L^{-1}]$ is the specific storage coefficient defined as $S_s = 1/\rho_f \, \partial\rho\phi/\partial h$. Note that this (standard) definition of S_s allows us to separate head (compressibility) and concentration dependencies of fluid mass ($\rho\phi$).

[15] Salt mass conservation is expressed by the advection-dispersion equation

$$\begin{aligned} \frac{\partial(\rho\phi\omega)}{\partial t} &= \omega\rho_f S_s \frac{\partial h}{\partial t} + \rho_f \phi \left(1 + 2\epsilon \frac{\omega}{\omega_s}\right) \frac{\partial \omega}{\partial t} \\ &= \nabla \times (\mathbf{u}\,\omega) - \nabla \times (\mathbf{D}\nabla\omega), \end{aligned} \tag{4}$$

where $\mathbf{D}[ML^{-1}T^{-1}]$ is a mass flux hydrodynamic diffusion-dispersion tensor $\mathbf{D} = (\mathbf{D}_0 + \phi\rho D_f \mathbf{I})$, equal to ρ times the conventional hydrodynamic dispersion tensor, where D_f $[L^2T^{-1}]$ is the molecular diffusion coefficient, $\mathbf{I}$ the identity matrix, and $\mathbf{D}_0$, similarly to $\mathbf{D}$, is a mass flux mechanical dispersion tensor, defined in terms of α_L $[L]$ and α_T $[L]$, longitudinal and transverse dispersivities, respectively, and $\mathbf{u}$, instead of $\mathbf{q}/\phi$.

[16] Boundary and initial conditions are required for solving equations (3) and (4). A known flux with a zero salt fraction is prescribed at the inland boundary. The shore is often represented by imposing a freshwater head equivalent to a zero saltwater head for flow and an advective flux condition (Adv.SF) for transport. This implies that the salt mass fraction equals that of seawater (ω_s) for inflowing portions of the boundary or equals that of the resident mass fraction for outflowing portions [see, e.g., *Voss and Souza*, 1987; *Frind*, 1982]. The bottom boundary is usually assumed as no flow of both salt and water [see, e.g., *Hidalgo et al.*, 2009]. The top boundary is often represented by a recharge or a free surface boundary condition (see discussion by *Chen et al.* [2010] and *Bear et al.* [2010]). Later, in sections 3.1 and 3.2, we will see that the type of boundary condition adopted is not important for the purposes of our work.

2.2. Vertically Averaged Flow Equation

[17] Vertical averaging basically entails integrating all variables along the z coordinate and dividing by the aquifer thickness. Vertical averaging and integration enjoy a long-standing tradition in practical hydrogeology because most groundwater observations are either vertically averaged (e.g., heads, concentrations) or integrated (e.g., transmissivity) [see, e.g., *De Wiest and Bear*, 1969; *Pinder and Celia*, 2006]. *Bear* [1972] explains in detail the method and some of the typical simplifications. For the sake of completeness, we outline below the derivation. For the sake of simplicity, we assume a confined aquifer, so as to avoid complications arising from the nonlinearity associated with variations in thickness of unconfined aquifers or from the phreatic level boundary conditions. However, we do so without loss of generality, because most of the above complications are associated with the flow equation, whose integration is not particularly sensitive to density dependence, as shown below.

[18] The vertical average of a function a is defined as

$$\bar{a}(x,y) = \frac{1}{b(x,y)} \int_{z_b(x,y)}^{z_t(x,y)} a(x,y,z)\, \mathrm{d}z, \tag{5}$$

where $z_b(x,y)$ and $z_t(x,y)$ are the vertical elevations of the bottom and top of the aquifer at (x,y), and $b(x,y) = (z_t - z_b)$ is the thickness of the aquifer, assumed subhorizontal (i.e., actual distances equal to horizontal distances, $\cos\theta = 1$, where θ is the aquifer slope, but vertical distances are still relevant for buoyancy forces).

[19] Averaging the flow equation (3), using the Leibnitz rule for handling spatial derivatives, yields

$$\rho_f S_s \frac{\partial \bar{h}}{\partial t} + \frac{\rho_f \epsilon}{\omega_s} \phi \frac{\partial \bar{\omega}}{\partial t} = \nabla_h \times \overline{\mathbf{u}_h} + R, \tag{6}$$

where the subscript h stands for (sub)horizontal, i.e., $\nabla_h = (\partial/\partial x, \partial/\partial y)$ and $\mathbf{u}_h = \rho(q_x, q_y)^T$. Note that the resulting differential equation is fluid mass conserving by construction. The source term $\boldsymbol{R}$ is

$$R = \frac{1}{b}\left[u_z(z_t) - u_z(z_b) + \mathbf{u}_h(z_b) \times \nabla_h z_b - \mathbf{u}_h(z_t) \times \nabla_h z_t\right], \tag{7}$$

which represents the total inflow per unit horizontal area (recharge) across the top and bottom boundaries.

2.3. Vertically Averaged Darcy's Law

[20] We assume that permeability (and therefore freshwater hydraulic conductivity) is homogeneous. Horizontal variations can be incorporated without difficulties. However, vertical variations are hard to accommodate. For instance, a high K zone will enhance seawater penetration if well connected to the sea at depth, but will hinder it, otherwise. The mixing zone tends to lie close to the bottom of high K zones [*Abarca*, 2006]. These examples show that the problem is highly nonlocal, so that a rigorous derivation will require nontrivial simplifications. Yet, *Abarca* [2006] and *Held et al.* [2005] also showed that an equivalent homogeneous medium reproduces quite well seawater intrusion patterns, provided that the variance or the correlation distance of ln K are moderate.

[21] First, we average the vertical component, which yields

$$\begin{aligned}\bar{q}_z &= \frac{-1}{(z_t - z_b)} \int_{z_b}^{z_t} K\left(\frac{\partial h}{\partial z} + \epsilon \frac{\omega}{\omega_s}\right) \mathrm{d}z \\ &= -\frac{K}{(z_t - z_b)}\left[h_t - h_b + \epsilon(z_t - z_b)\frac{\bar{\omega}}{\omega_s}\right].\end{aligned} \tag{8}$$

Therefore,

$$h_b = h_t + \epsilon(z_t - z_b)\frac{\bar{\omega}}{\omega_s} + \frac{\bar{q}_z(z_t - z_b)}{K}, \tag{9}$$

where the subscripts b and t stand for the bottom and top of the aquifer.

[22] We now integrate the horizontal component of flux and use the Leibnitz rule to get

$$\begin{aligned}\bar{q}_h b &= -K \int_{z_b}^{z_t} \nabla_h h \, \mathrm{d}z \\ &= -Kb\,\nabla_h \bar{h} - K\left[(\bar{h} - h_t)\nabla_h z_t + (h_b - \bar{h})\nabla_h z_b\right].\end{aligned} \tag{10}$$

Using (9) to eliminate h_b and terming $Kb = T$, leads to

$$\bar{q}_h b = -T\left[\nabla_h \bar{h} + \left(\frac{\bar{q}_z}{K} + \epsilon\frac{\bar{\omega}}{\omega_s}\right)\nabla_h z_b + \frac{(\bar{h} - h_t)}{b}\nabla_h b\right], \tag{11}$$

where the second and third terms are zero if the aquifer bottom is horizontal and the thickness is constant. Under such conditions, Darcy's law is independent of density variations. This may sound paradoxical, as one might expect the flux to depend on density gradients [see, e.g., *Sorek et al.*, 2001]. Actually, it simply reflects that for buoyancy to affect averaged flow, the aquifer must display some slope, either in the mean or in the bottom elevations.

[23] Since the state variables of the problem are $\bar{h}$ and $\bar{\omega}$, practical application of equation (11) requires approximating $\bar{q}_z$. In general, $\bar{q}_z$ will not be zero both because the mean elevation of the aquifer does not need to be horizontal, independent of density variations, and because of the vertical component of seawater flux (Figure 1). The first component of $\bar{q}_z$, associated to variations of aquifer elevation, can be neglected without loss of generality, as it is done in usual aquifer studies because of the subhorizontality assumption and because, in practice, it is implicit in the actual measurements of transmissivity. The second one, associated to density differences, can be considered to be of subleading order with respect to horizontal fluxes in regional aquifers and also neglected (in Appendix B we will see that it may be relevant for the local analysis of seawater intrusion if transverse dispersivity is large). Neglecting $\bar{q}_z$ facilitates approximating the last term of equation (11) because the pressure is hydrostatic. Therefore, equivalent freshwater head is constant above the interface z_I (Figure 2) and, assuming constant salinity ($\omega = \omega_s$) grows linearly with depth below ($h = h_t + \epsilon[z_I - z]$). Averaging and realizing that $\bar{\omega}/\omega_s = (z_I - z_b)/(z_t - z_b)$ yields

$$\frac{\bar{h} - h_t}{b} = \frac{\epsilon}{2}\left(\frac{\bar{\omega}}{\omega_s}\right)^2. \tag{12}$$

A more complex expression for this term assuming a mixing zone is derived in Appendix B. Preliminary calculations showed that the expression in Appendix B is required for separating seawater and freshwater fluxes, which will be required later. But equation (12) is sufficient to compute the mean flux. Therefore, the averaged Darcy's law is written as

$$\bar{q}_h b = -T\left[\nabla_h \bar{h} + \epsilon\frac{\bar{\omega}}{\omega_s}\nabla_h z_b + \frac{\epsilon}{2}\left(\frac{\bar{\omega}}{\omega_s}\right)^2 \nabla_h b\right]. \tag{13}$$

2.4. Vertically Averaged Transport Equation

[24] To average the transport equation (4) we use the same approach as for the flow equation. Regarding the storage term, we separate the dependence of ($\rho\phi$) on head and concentration while assuming that the time fluctuations of pressure are constant along the vertical. After combining terms, this leads to

$$\begin{aligned}&\bar{\omega}\rho_f S_s \frac{\partial \bar{h}}{\partial t} + \phi\rho_f\left(\frac{\partial \bar{\omega}}{\partial t} + \frac{\epsilon}{\omega_s}\frac{\partial \overline{\omega^2}}{\partial t}\right) \\ &= \nabla_h \times \overline{\mathbf{u}_h \omega} - \nabla_h \times \left(\overline{\mathbf{D}\nabla_h}\right) + R^*,\end{aligned} \tag{14}$$

where the source term R^* is identical to R (equation (7)), but with the salt mass flux ($\mathbf{u}\omega - \mathbf{D}\nabla_h\omega$) instead of $\mathbf{u}$. It represents the total salt flux across the top and bottom of the aquifer.

[25] In order to evaluate the effect of vertical fluctuations in flux and concentration, the fluid density (included in the

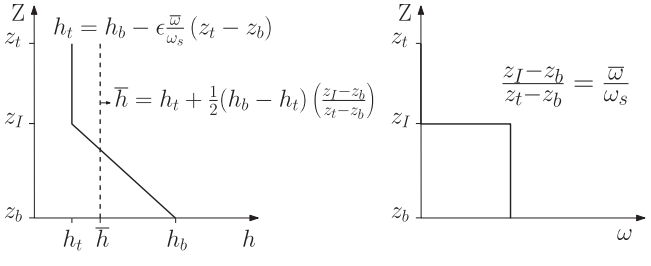

Figure 2. Equivalent freshwater head and salt mass fraction profiles under the sharp interface approach and neglecting $\bar{q}_z$.

mass flux hydrodynamic diffusion-dispersion tensor), the salt mass fraction, and fluid mass flux are decomposed into their mean values and fluctuations about them

$$\mathbf{D} = \overline{\mathbf{D}} + \mathbf{D}', \quad \omega = \bar{\omega} + \omega', \quad \mathbf{u} = \overline{\mathbf{u}} + \mathbf{u}', \tag{15}$$

where $\mathbf{u}'$, $\mathbf{D}'$, and ω' denote the fluctuations about the mean of the fluid mass flux, the mass flux hydrodynamic dispersion tensor, and the salt mass fraction, respectively. These equations are substituted in (14). To evaluate $\overline{\omega^2}$, we approximate ω again as in Figure 2, so that $\omega = \omega_s$ in the lower $\bar{\omega}/\omega_s$ fraction of the aquifer and $\omega = 0$ in the upper portion. Therefore, $\overline{\omega^2} = \bar{\omega}\omega_s$, which yields

$$\begin{aligned} \bar{\omega}\rho_f S_s \frac{\partial \bar{h}}{\partial t} + \phi\rho_f(1+\epsilon)\frac{\partial \bar{\omega}}{\partial t} &= \nabla_h \times \overline{\mathbf{u}_h}\,\bar{\omega} + \nabla_h \times \overline{\mathbf{u}_h'\,\omega'} \\ &- \nabla_h \times (\overline{\mathbf{D}}\,\nabla_h\bar{\omega}) - \nabla_h \times (\overline{\mathbf{D}'\,\nabla_h\omega'}) + R^*. \end{aligned} \tag{16}$$

Sorek et al. [2001] estimated the fourth term of the right-hand side of (16), verifying that it is much smaller than the product of the averaged terms. Thus, it can be neglected. However, the second term of the right-hand side of (16) is probably large because, at least under natural conditions, perturbations on $\mathbf{u}'$ and ω' are likely to be correlated: salt water ($\omega' > 0$) flows inland ($\mathbf{u}' < 0$) while freshwater ($\omega' < 0$) flows seaward ($\mathbf{u}' > 0$), see the bottom of Figure 1. Strictly speaking, $\overline{\mathbf{u}_h'\,\omega'}$ is a dispersion term because it represents the effect of fluctuations in velocity over the transport of mean concentration. As we mentioned in the introduction, it is natural to conjecture that it can be approximated by a Fickian dispersion term because of the tradition in stochastic hydrology. That is, $\overline{\mathbf{u}_h'\,\omega'} = \mathbf{D}^*\,\nabla_h\bar{\omega}$, where $\mathbf{D}^*$ is the mass flux hydrodynamic dispersion tensor emerging from velocity fluctuations. In Appendix A, we show that, indeed, the approximation is appropriate, but only for horizontal aquifer bottoms. If the bottom is irregular, an additional sink-source term, $r(x)$, is needed. The resulting averaged transport equation is

$$\begin{aligned} &\bar{\omega}\rho_f S_s \frac{\partial \bar{h}}{\partial t} + \phi\rho_s \frac{\partial \bar{\omega}}{\partial t} \\ &\quad = \nabla_h \times \overline{\mathbf{u}_h}\,\bar{\omega} - \nabla_h \times \left[\left(\overline{\mathbf{D}} + \mathbf{D}^*\right)\nabla_h\bar{\omega}\right] + R^* + r, \end{aligned} \tag{17}$$

where we have used the fact that seawater density ρ_s equals $\rho_f(1+\epsilon)$ and the additional mass flux hydrodynamic dispersion tensor, $\mathbf{D}^*$, defined by (A7), is used to represent the inland flow of seawater. Moreover, a zero mean sink-source term, $r(x)$, may be needed when the aquifer bottom is irregular and, therefore, $\bar{\omega}$ is not smooth. In practice, equation (A7) is not easy to evaluate. We assume that $\mathbf{D}^*$ can be approximated as

$$D_{ij}^* = \left[\delta_{ij}\alpha_T^*|\overline{\mathbf{u}}| + \left(\alpha_L^* - \alpha_T^*\right)\frac{\overline{u_i}\;\overline{u_j}}{|\overline{\mathbf{u}}|}\right], \tag{18}$$

where α_L^* and α_T^* are effective dispersivities. They are obtained by computing $J_d(x) = \overline{\mathbf{u}_h'\,\omega'}$ and, then, ensuring that $J_d(x) = \mathbf{D}^*\,\nabla_h\bar{\omega}$, which leads to

$$\alpha_L^* = \frac{J_{di}\overline{u_i} + J_{dj}\overline{u_j}}{|\overline{\mathbf{u}}|\left(\overline{u_i}\,\partial_i\bar{\omega} + \overline{u_j}\,\partial_j\bar{\omega}\right)}, \quad i,j = x,y, \tag{19}$$

$$\alpha_T^* = \frac{J_{di}\,\overline{u_j} - J_{dj}\,\overline{u_i}}{|\overline{\mathbf{u}}|\left(\overline{u_j}\,\partial_i\bar{\omega} - \overline{u_i}\,\partial_j\bar{\omega}\right)}, \quad i,j = x,y. \tag{20}$$

[26] Boundary conditions are in general the vertically integrated equivalents of the fully dimensional models, except at the shore. In the vertically integrated models, salt flux is simulated by dispersion with the result that an advective flux condition would not work and salt mass fraction must be prescribed (Dirichlet boundary condition) to the value of the average concentration at the shore.

3. Numerical Solution and Validation

[27] The proposed equations can be solved with any conventional 1- or 2-D density-dependent flow and transport code. The only requirements are that Darcy's law includes a term projecting buoyancy forces on to the aquifer bottom slope (second term in equation (13)), can be modified to include the aquifer thickness gradient term (third term in equation (13)), and optionally, the vertical fluxes term in equation (11), which we have neglected here.

[28] The only potential difficulty lies in the evaluation of the upscaled dispersivities (equations (19) and (20)), which require having computed $\overline{\mathbf{u}_h'\,\omega'}$. To evaluate this term, a simplified profile of ω and $\mathbf{u}$ as a function of z (such as those in Figure 1) must be obtained from the vertically averaged variables ($\overline{\mathbf{u}}, \bar{\omega}, \bar{h}$). Actual application to complex real problems requires code development that fall beyond the scope of this paper. Still, we present a simple algorithm in Appendix B to show that the problem is not complex from a conceptual point of view. In essence, it entails splitting $\mathbf{u}$ and h into their freshwater and seawater portions, above and below the mixing zone, z_I (see Figure 1), which is obtained from $\bar{\omega}$. The resulting profiles are used to compute $\overline{\mathbf{u}_h'\,\omega'}$, which allows computing dispersivities (equations (19) and (20)). These are used to recompute $\bar{h}$ and $\bar{\omega}$, and the procedure is repeated until convergence is reached. As shown in Appendix B, the algorithm can be programmed in a spreadsheet for 1-D steady state problems.

[29] We have also solved fully dimensional models to validate the Fickian approximation of the saltwater flux (and also to compare with the dimensionally reduced solution). Fluctuations and mean mass flux and salt mass fractions are obtained along vertical strings of nodes. These values are used for computing the additional dispersion term $\mathbf{D}^*$, equation (18). The resulting dispersivities are added to the local ones in the equivalent dimensionally reduced models.

[30] In the following, we test the validity of the equations derived in section 2 in three 2-D vertical cross sections and one 3-D sloping aquifer. We evaluate the fit between fully and dimensionally reduced results. All comparisons concern steady state and confined aquifers. Thus, R and R^* are zero in equations (6) and (17), respectively.

3.1. 2-D Models - 1-D Equivalent Models

[31] Three geometries of a confined aquifer were studied (Figure 3). The first one is the dispersive Henry problem [*Abarca et al.*, 2007a], case (a) in Figure 3. This problem is a generalization of the traditional diffusive Henry problem [*Henry*, 1964] to ensure realistic salinity profiles. Since conventional seawater intrusion benchmarks assume a

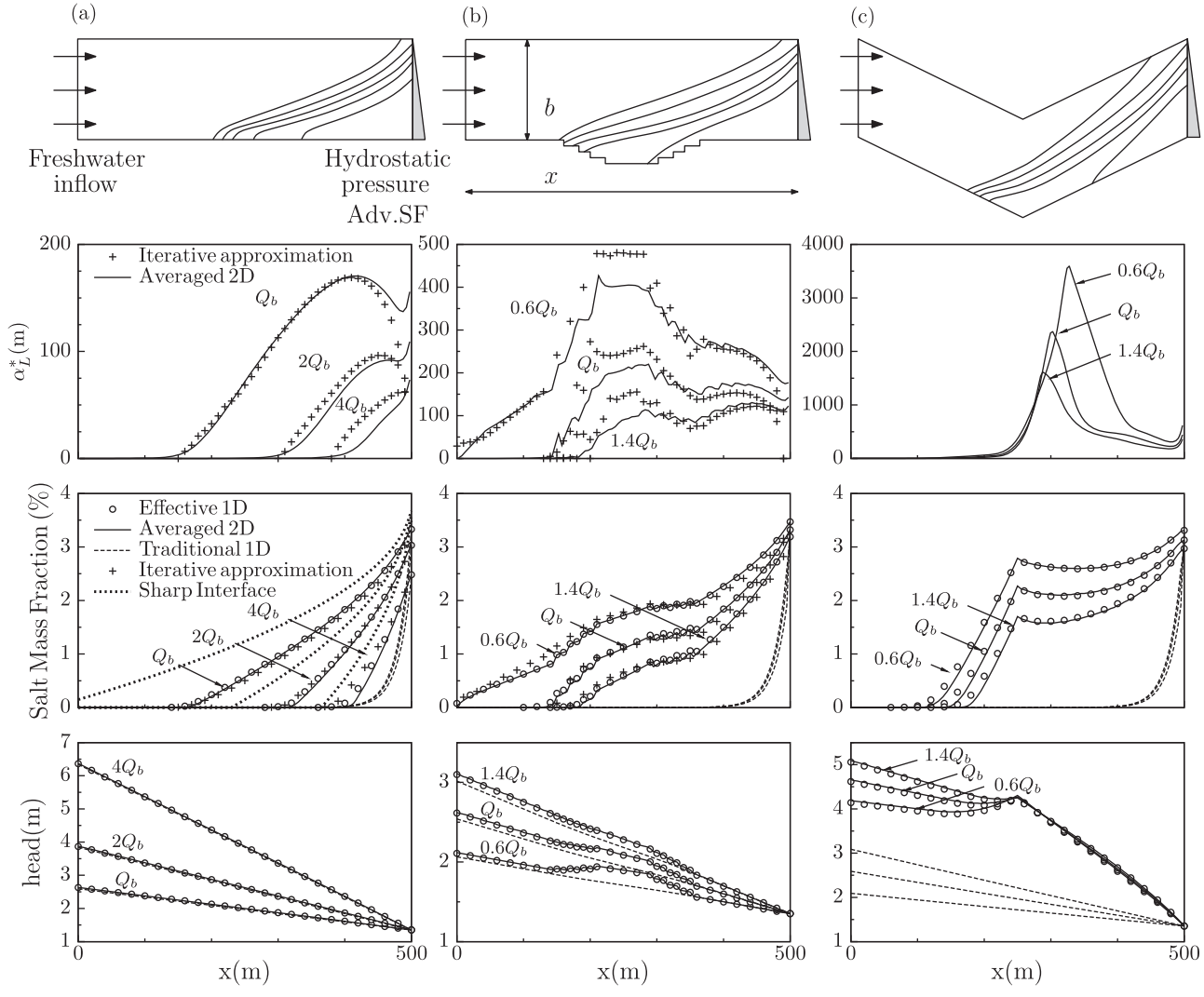

Figure 3. Schematic descriptions of the numerical 2-D cross-section models. Seawater head is prescribed at the sea boundary, where salt mass flux is prescribed to be advective, Adv.SF ($\mathbf{u} \times \mathbf{n}\,\omega|_{x=L}$ where water exits the aquifer, and $\mathbf{u} \times \mathbf{n}\,\omega_s$ where it enters). Isoconcentration lines of 95%, 75%, 50%, 25%, and 10% isochlors for a constant freshwater inflow of $Q_b = 25$ m^3 d^{-1} m^{-1}. Effective dispersivities and the zero mean sink-source used for the equivalent 1-D models for the different constant freshwater inflow values, and those calculated from the proposed iterative algorithm. The sink-source term takes the form of sequence dipoles (one at each step) for case (b) and a single mass injection at the deepest point of the aquifer and a distributed extraction toward the sea for case (c). Finally, we show a comparison between the averaged salt mass fraction and equivalent freshwater head results of the averaged 2-D model (thick solid lines), the solution of the traditional 1-D model (dashed lines), and the solution of the equivalent, vertically integrated 1-D model (open circles) for the different constant freshwater inflow values, as well as results from the iterative algorithm (crosses) and sharp interface results.

horizontal aquifer bottom, two other geometries were employed to study the effects of irregularities in the aquifer topography, so as to provide more complex tests of the proposed methodology. In case (b) Figure 3, the aquifer top is flat, but the bottom varies stepwise, which leads to discontinuous mean concentrations. The thickness is constant in case (c) Figure 3. Flow and transport parameters used for the models are listed in Table 1. We have solved the equations with code TRANSDENS [*Hidalgo et al.*, 2005].

[32] Boundary conditions are identical for the three models. A constant flow rate ($Q_b = 25$ m^3 d^{-1} m^{-1}) of

Table 1. Parameters Used in the Simulations

Parameter	Value	
X	500 m	Domain length
B	100 m	Domain thickness
K	1.18e-10 m^2	Permeability (isotropic)
α_L	α_L 10 m	Longitudinal dispersivity
α_T	α_T 1 m	Transverse dispersivity
D_m	1.0e-9 m^2 s^{-1}	Molecular diffusion coefficient
μ	0.001 kg ms^{-1}	Freshwater viscosity
ϕ	0.2	Porosity
$\in$	0.027	Density contrast parameter

freshwater (with a salt mass fraction equal to $\omega = 0$ kg kg^{-1}) is imposed along the inland boundary. Seawater hydrostatic pressure is prescribed along the seaside boundary and the Adv.SF boundary condition is adopted for transport. The remaining boundaries are closed to flow and solute transport.

[33] The results are shown in Figure 3. Upscaled dispersivities do indeed reflect the increase in dispersion required to represent the seawater influx in the dimensionally reduced (l-D) models. In fact, the dispersivities calculated tend to increase with seawater penetration.

[34] In addition to dispersion, the zero mean sink-source term, r in equation (17), needs to be activated in cases (b) and (c). Geometrical irregularities cause nonuniform mean concentration gradients, which cannot be represented by a Fickian dispersion term (the dispersion coefficient would lead to negative dispersivities, which is computationally inconvenient and conceptually puzzling). In case (b), $\mathbf{D}^*$ is approximated by interpolation from neighboring points at each step and $r(x)$ takes the form of a sequence of dipoles (one at each step) with a strength that is proportional to $\mathbf{D}^*\Delta\bar{\omega}$, where $\Delta\bar{\omega}$ is the jump in mean concentration (equation (A10)). In case (c), $r(x)$ consists of a single mass injection (at the deepest point of the aquifer) of strength that is proportional to the jump in concentration gradients, and a distributed extraction toward the sea in the region where $\nabla_h\bar{\omega}$ is negative so as to ensure a zero mean $r(x)$ (see Figure 3). Details of the procedure are discussed in Appendix A.

[35] Computed mean mass fractions and equivalent freshwater heads using the vertically averaged model (open circles) are virtually identical to those obtained by averaging the solution of the fully dimensional model (thick solid lines). In contrast, the solution obtained with a traditional l-D approximation (i.e., using the same equations as in the effective l-D model, but without upscaling dispersion) leads to very inaccurate results, underestimating penetration. Therefore, we conclude that the proposed equations, though simple, capture the essential dynamics of the seawater recirculation.

[36] It is worth noticing that the solution is not overly sensitive to the precise value of $\mathbf{D}^*$. The solutions obtained with the spreadsheet approximation of Appendix B (crosses in cases [a] and [b]) are quite accurate, despite the fact that the estimated dispersivities are somewhat high. This suggest that, whereas upscaling dispersion is critical, small errors in $\mathbf{D}^*$ do not translate into large errors of either computed mean mass fraction or, much less, heads.

Table 2. Parameters Used in the 3-D Sloping Aquifer

Parameter	Value	
K	1.25e-11 m^2	Permeability (isotropic)
$\alpha_{L\max}$	10 m	Max. longitudinal dispersivity
$\alpha_{L\mathrm{med}}$	10 m	Med. longitudinal dispersivity
$\alpha_{L\min}$	1 m	Min. longitudinal dispersivity
α_T	1 m	Transverse dispersivity
D_m	1.0e-9 m^2 s^{-1}	Molecular diffusion coefficient
μ	0.001 kg ms^{-1}	Freshwater viscosity
ϕ	0.2	Porosity
$\in$	0.027	Density contrast parameter

3.2. 3-D Model - 2-D Equivalent Areal Model

[37] A confined aquifer with a lateral slope (1%) is chosen to validate the proposed equations. This case was proposed by *Abarca et al.* [2007b] to study the effect of variation in aquifer bathymetry. The size of the model is $3000 \times 1500 \times 50$ m^3 (see Figure 4). Owing to the symmetry with respect to the y-axis, numerical calculations are carried out in one half of the aquifer. To avoid numerical dispersion, the vertical discretization is fine compared with the horizontal one.

[38] The boundary conditions (Figure 4) are: constant freshwater inflow from inland ($Q_b = 214$ m^3 d^{-1} with $\omega = 0$ kg kg^{-1}), specified pressure along the seaside boundary ($p = \rho_s g z$), and the Adv.SF boundary condition for transport. The remaining boundaries are closed to flow and solute transport. The aquifer parameters are given in Table 2. The computer simulations were performed with SUTRA [*Voss and Provost*, 2002].

[39] The effective dispersivities, computed with equations (19) and (20), are shown in Figure 5. They are largest in the region adjacent to the sea and in the deepest portion of the aquifer, diminishing further inland. Note also, the relatively large values of α_T.

[40] The effective 2-D model (see Figure 6) accurately reproduces both equivalent freshwater head and salt mass fraction distributions of the 3-D model. In contrast, the traditional 2-D areal model (i.e., without upscaling dispersion) leads to a much narrower mixing zone, far shorter saltwater penetration (50% isochlor), and misses the lateral convection cell in the saltwater wedge. Therefore, we conclude again that upscaling dispersion is required for the effective

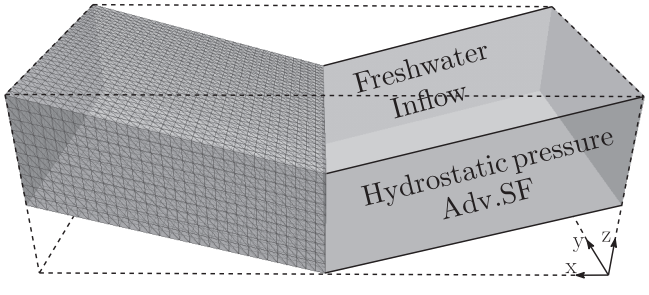

Figure 4. A schematic description of a laterally sloping confined aquifer. A 3-D model and boundary conditions shows freshwater flows from the background (inland) toward the foreground (seaside).

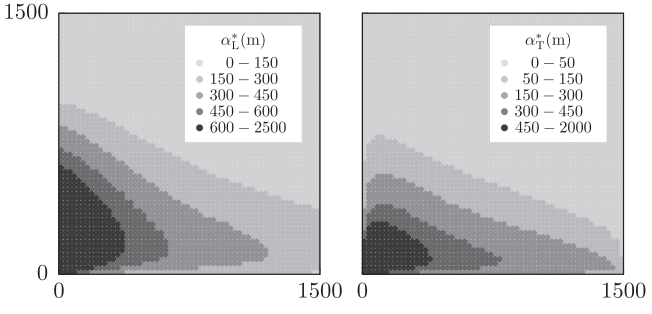

Figure 5. The distribution of the longitudinal and transverse effective dispersivities for each element from the fluctuations about the spatial mean flow and concentration.

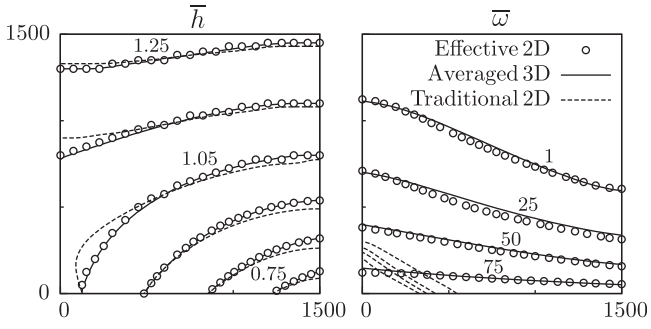

Figure 6. A plan view of the equivalent freshwater head (a) and salt mass fraction distribution (b) for the averaged 3-D model (thick solid lines) compared with the traditional 2-D areal model (dashed lines), and the effective 2-D areal model (circles). When the additional dispersion term is included, the effective 2-D areal model approximates to the 3-D dynamics with satisfactory results.

2-D areal model to approximate the 3-D dynamics. The agreement between the two models indicates that the effects of vertical fluxes may be represented by a Fickian dispersion term, and that the dynamics of seawater intrusion in a 3-D system may be captured very well by effective dimensionally reduced equivalent models.

[41] Several sets of simulations were carried out to test mass balance accuracy by increasing the value of freshwater inflow. *Smith* [2004] studied the role of the quantification of the saltwater mass flux (SMF) in seawater intrusion studies with velocity dependent dispersion. He found that saltwater flux depends on the geometric average of the principal components of hydraulic conductivity and on the square root of the transverse dispersivity. This was further tested by *Abarca et al.* [2007a], who showed that seawater flux is essentially proportional to the geometric average of the hydraulic conductivity and $(\alpha_T)^{1/3}$, and independent of the freshwater flux from inland.

[42] The resulting behavior of SMF, illustrated in Figure 7, indicates that prescribed freshwater flux plays a major role. In fact, SMF depends nonmonotonically on freshwater flux. In the absence of prescribed freshwater flux, SMF would be zero because the aquifer would fill with saltwater.

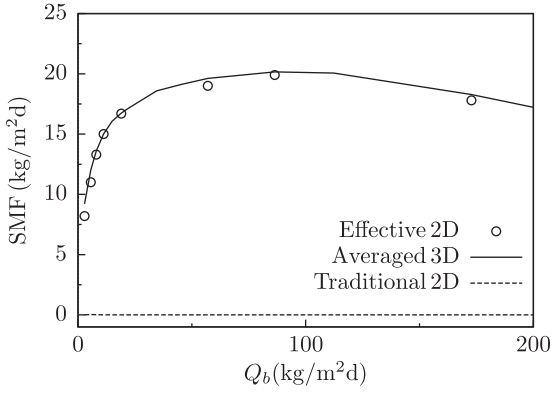

Figure 7. Salt mass flux (kg s^{-1}) results from the 3-D model (thick solid lines), the effective 2-D areal model (circles), and from the traditional 2-D areal model (dashed lines) for different freshwater inflow values from inland (Q_b).

The prescribed freshwater flux increases, as do the pressure gradients close to the seaside boundary and the dispersion coefficient. Therefore, SMF increases although the interface rotates and retreats seaward. This dependence is maintained while most of the seaside boundary is occupied by seawater. If this does not occur, further increases in freshwater inflow results in a parallel seaward retreat of the mixing zone and in a slight reduction in SMF. Figure 7 shows that, in contrast to the traditional model, the effective 2-D areal model reflects such behavior.

[43] Finally, we test the dimensionally reduced formulation on a pumping scenario. Constant freshwater inflow from inland was $Q_b = 600$ m^3 d^{-1}, and a fully penetrating well at a distance $L_w = 750$ m from the coast pumps a rate Q_w that is gradually increased ($Q_w/Q_b = 0.2 - 1$).

[44] Figure 8 displays the results. As in the unpumped case, the proposed vertically integrated model accurately reproduces the fully dimensional model results, while the traditional 2-D model does not. Saltwater penetration is shorter and pumped water salinity lower in the 2-D traditional model than in the 3-D model. Moreover, the traditional 2-D models yield an unrealistically sharp seawater intrusion wedge. The vertically averaged salinity computed with the proposed approach reproduces much better the smooth transition zones typically observed in actual seawater intrusion problems [e.g., *Iribar et al.*, 1997; *Vazquez-Sune et al.*, 2006].

4. Summary and Conclusions

[45] A vertically integrated formulation was developed for modeling regional seawater intrusion. We demonstrate that vertical integration should include the impact of the fluctuations about the spatial mean mass flux ($\mathbf{u}'$) and salt mass fraction (ω') in the governing equations to take into account the effects of mixing mechanisms induced by vertical fluctuations in horizontal fluxes. The dimensionally reduced formulation correctly reflects the effective dynamics in a 3-D system.

[46] The resulting equations are similar to a plain dimensional reduction of the original 3-D equations with some additional terms. Two additional terms are required in Darcy's law: one representing the slope of the aquifer bottom and the other the variations in aquifer thickness. As for transport, a dispersion term must be added to represent the inland flux of salt. A Fickian dispersion with enhanced dispersivity near the coast is sufficient whenever the aquifer geometry is regular. However, an additional zero mean sink-source term is necessary if the geometry of the aquifer is irregular. Step changes in thickness can be accommodated by mass dipoles, whereas the injection-extraction of mass must be distributed in cases where the slope of the aquifer is irregular.

[47] The accuracy of this formulation is validated by comparing the direct steady state numerical simulations of the fully dimensional and the dimensionally reduced problems. The traditional dimensionally reduced models (i.e., without upscaling dispersion) cannot accurately depict the effective dynamics in a 3-D system. They produce much shorter and sharper seawater intrusion wedges than observed in reality. Our effective formulation produces rather accurate agreements in terms of head and salt mass fraction distributions. We conclude that the additional

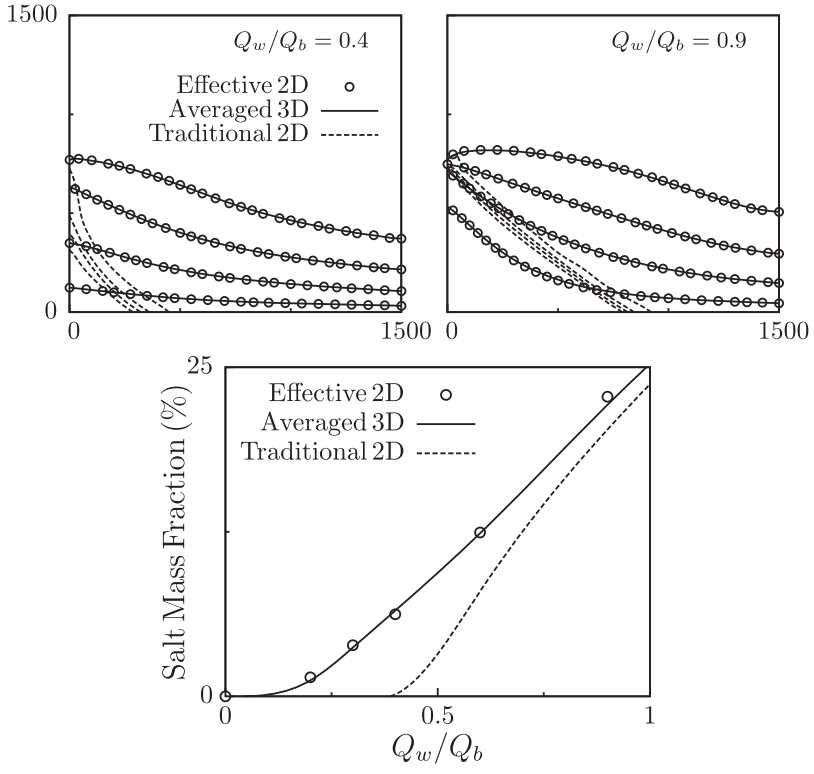

Figure 8. A plan view of the salt mass fraction distribution considering a fully penetrating well at a distance of 750 m from the coast for different pumping rates ($Q_w/Q_b = 0.4$ and 0.9). The thick solid lines represent the averaged 3-D model, the dashed lines represent the traditional 2-D areal model, and the circles represent the effective 2-D areal model. Salinity at the pumping well in the 3-D model, the effective 2-D areal model, and the traditional 2-D areal model for different pumping rates.

dispersion term to represent the mixing mechanisms induced by vertical fluctuations in horizontal fluxes allows for a realistic and an efficient modeling of seawater intrusion in coastal aquifers by means of 2-D areal models.

Appendix A: Perturbation Analysis

[48] Inserting (15) into (4) yields

$$\begin{aligned}&\nabla\times\overline{\mathbf{u}}\,\bar{\omega}+\nabla\times\mathbf{u}'\bar{\omega}+\nabla\times\overline{\mathbf{u}}\,\omega'+\nabla\times\mathbf{u}'\omega'\\&-\nabla\times\overline{\mathbf{D}}\nabla\bar{\omega}-\nabla\times\mathbf{D}'\nabla\bar{\omega}-\nabla\times\overline{\mathbf{D}}\nabla\omega'-\nabla\times\mathbf{D}'\nabla\omega'=0.\end{aligned}\tag{A1}$$

Averaging (A1) gives (16). Subtracting the mean equation (16) from (A1) and disregarding terms that are quadratic in the fluctuations and source terms that contain spatial derivatives of an order higher than one yields

$$\nabla\times\overline{\mathbf{u}}\,\omega'-\nabla\times\overline{\mathbf{D}}\nabla\omega'=-(\mathbf{u}_h)'\times\nabla_h\bar{\omega}.\tag{A2}$$

The Green theorem allows solving (A2) as

$$\omega'(x)=-\int g(\mathbf{x}|\mathbf{x}')\,\mathbf{u}_h'(\mathbf{x}')\,\nabla_h'\bar{\omega}(x')d\mathbf{x}',\tag{A3}$$

where the Green function $g(\mathbf{x}|\mathbf{x}')$ denotes the solution of (A2) for the source term $\delta(\mathbf{x}-\mathbf{x}')$. Thus, the third term in (16) can be written formally as

$$\nabla_h\times\overline{\mathbf{u}_h'\,\omega'}\equiv\nabla_h\times J_d(x)=\nabla_h\times\int\mathbf{C}(x,x')\nabla_h'\bar{\omega}(x')dx'.\tag{A4}$$

This term represents a nonlocal dispersive flux, where $\mathbf{C}(x,x')$ is defined by

$$\mathbf{C}(x,x')\equiv\int\overline{g(\mathbf{x}|\mathbf{x}')\,\mathbf{u}_h'(x)\otimes\mathbf{u}_h'(\mathbf{x}')}dz'.\tag{A5}$$

We assume that $\mathbf{C}(x,x')$ is small for large deviations $|x-x'|$. Thus, (A4) can be localized according to

$$\nabla_h\times J_d(x)=\nabla_h\times\left[\int\mathbf{C}(x,x')\,dx'\right]\nabla_h\bar{\omega}(x).\tag{A6}$$

We define the term in the square brackets as

$$\int\mathbf{C}(x,x')\,dx'\equiv\mathbf{D}^*.\tag{A7}$$

[49] Note that this localization is based on the assumption that $\mathbf{C}(x,x')$ is small for $|x-x'|$ large and that $\bar{\omega}(x)$ is a smooth function of x. Inserting the latter in (16), the averaged transport equation yields (17). The validity of this approximation is tested numerically (equations (18)–(20)). Accordingly, it works well whenever the aquifer bathymetry and thus $\bar{\omega}$ are smooth. Otherwise, additional source terms appear in the localization of (A4) as outlined below. Two cases must be addressed (Figure A1). If the aquifer bottom displays a step jump, $\bar{\omega}$ will be discontinuous. If the aquifer bottom displays sharp irregularities, $\bar{\omega}$ will be

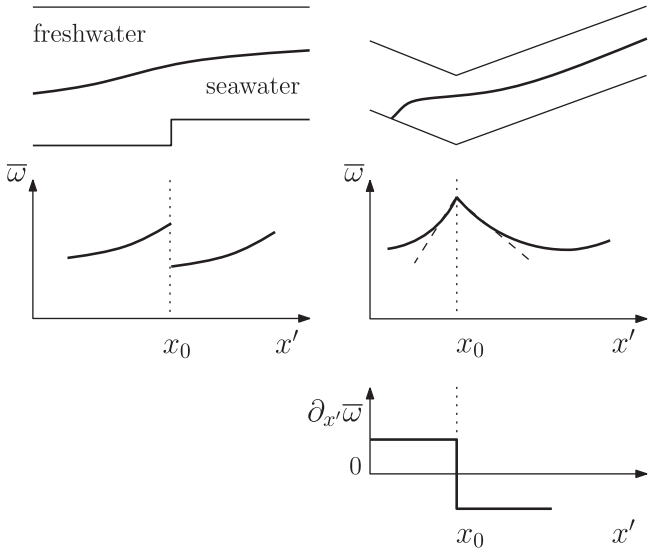

Figure A1. A comparison of the sink-source term r for the cases where the bottom of the aquifer is irregular (cases [b] and [c]) and their qualitative approximation (equations (A10)–(A14)).

nonderivable. Neither type of solution can be represented by a localized dispersion term as (A6).

[50] In the case of a step jump in the aquifer bottom, expansion of the integral in (A4) in two spatial dimensions gives

$$\frac{\partial}{\partial x}J_d(x) = \frac{\partial}{\partial x}\times\left[\int_0^{x_0^-}\mathbf{C}(x,x')\frac{\partial}{\partial x'}\bar{\omega}(x')dx' + \int_{x_0^+}^{L}\mathbf{C}(x,x')\frac{\partial}{\partial x'}\bar{\omega}(x')dx' + \int_{x_0^+}^{x_0^-}\mathbf{C}(x,x')\frac{\partial}{\partial x'}\bar{\omega}(x')dx'\right], \tag{A8}$$

where we set $x_0^{\pm} = x_0 \pm \delta$ with δ a very short distance compared with the problem dimensions. Assuming that $\mathbf{C}(x,x')$ is continuous in x_0, the last term is the last term $\mathbf{C}(x,x_0)\Delta\bar{\omega}$, where $\Delta\bar{\omega} = \bar{\omega}^+ - \bar{\omega}^-$. The remaining integrals can be localized as in (A6). Thus, we obtain for (A8)

$$\frac{\partial}{\partial x}J_d(x) = \frac{\partial}{\partial x}\times\left[\mathbf{D}^*\frac{\partial}{\partial x}\bar{\omega}\right] + r, \tag{A9}$$

where r represents the jump in dispersive fluxes. Recognizing that $\mathbf{C}(x,x_0)$ is sharply peaked about x_0, thus, this term can be approximated by

$$r = \frac{\partial}{\partial x}\mathbf{C}(x,x_0)\Delta\bar{\omega} = A_0[\delta(x-x_0^-) - \delta(x-x_0^+)]\Delta\bar{\omega}. \tag{A10}$$

That is, the net effect of the step jump is a dipole at x_0, where A_0 is a constant that depends on $\mathbf{C}(x,x')$ (Figure A2). Inserting (A10) into (A9) to approximate $\overline{\mathbf{u}_h'\,\omega'}$ in equation (17) leads to the following averaged transport equation:

$$\frac{\partial}{\partial x}\times\overline{\mathbf{u}_h}\,\bar{\omega} - \frac{\partial}{\partial x}\times\left[\left(\overline{\mathbf{D}}+\mathbf{D}^*\right)\frac{\partial}{\partial x}\bar{\omega}\right] = A_0[\delta(x-x_0^-) - \delta(x-x_0^+)]\Delta\omega. \tag{A11}$$

In the second case of Figure A1, the derivative of $\bar{\omega}(x)$ is discontinuous at x_0 and negative between x_0 and x_1. Therefore, we approximate $\nabla_h\bar{\omega}(x)$ in $[x_0-\delta, x_1]$ as

$$\frac{\partial}{\partial x}\bar{\omega}(x) = a_0H(x_0-x) + a_1H(x-x_0), \tag{A12}$$

where a_0 and a_1 are the slopes of $\bar{\omega}(x)$ to the left and the right of x_0. We rewrite now the flux $J_d(x)$ tautologically by defining a sink-source term, $r(x)$, which is precisely the residual error between the original problem (A4) and the localized definition, yielding

$$r(x) = \frac{\partial}{\partial x}\int_0^L \mathrm{d}x'\mathbf{C}(x,x')\frac{\partial}{\partial x'}\bar{\omega}(x') - \frac{\partial}{\partial x}\mathbf{D}^*(x)\frac{\partial}{\partial x}\bar{\omega}(x). \tag{A13}$$

We assume that $r(x)$ is only of importance for $x \in [x_0-\delta, x_1]$ and otherwise the localized expression provides a good approximation. Thus, we restrict the term $r(x)$ to the interval $[x_0-\delta, x_1]$. In this interval, the derivative $\nabla_h\bar{\omega}(x)$ can be approximated by (A12). We also assume that $\mathbf{D}^*(x)$ varies only moderately within $[x_0-\delta, x_1]$ and set $\mathbf{D}^*(x) \approx \mathbf{D}^*_m = [\mathbf{D}^*(x_0) + \mathbf{D}^*(x_1)]/2$. Thus, we obtain for the second term in (A13)

$$r_2(x) \approx -\mathbf{D}^*_m(a_1-a_0)\delta(x-x_0). \tag{A14}$$

This term represents an injection of mass at $x = x_0$. For mass conservation reasons, the first term in (A13) should represent an extraction of the same amount of mass over

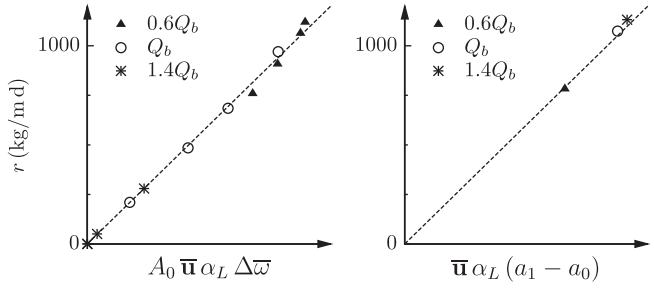

Figure A2. The averaged salt mass fraction and approximation of the derivative of $\bar{\omega}(x)$ in the cases where the bottom of the aquifer is irregular: step jump (left) or change in slope (right).

the interval $[x_0, x_1]$ (Figure A2). In order to verify this, we integrate $r_1(x)$ from x_0 to x_1. This gives

$$\begin{aligned}\int_{x_0}^{x_1} \mathrm{d}x\, r_1(x) &= \int_{x_0}^{x_1} \mathrm{d}x \frac{\partial}{\partial x'} \int_0^L \mathrm{d}x' \mathbf{C}(x,x') \frac{\partial}{\partial x'} \bar{\omega}(x') \\ &= \int_0^L \mathrm{d}x' \mathbf{C}(x_1,x') \frac{\partial}{\partial x'} \bar{\omega}(x') - \int_0^L \mathrm{d}x' \mathbf{C}(x_0,x') \frac{\partial}{\partial x'} \bar{\omega}(x') \\ &= \mathbf{D}_m^*(a_1 - a_0),\end{aligned} \tag{A15}$$

where the last two integrals can now be localized by taking into account that $\mathbf{C}(x_0, x')$ and $\mathbf{C}(x_1, x')$ are sharply peaked about x_0 and x_1, respectively. We have also used the fact that a_0 and a_1 are the slopes of $\bar{\omega}(x)$ in x_0 and x_1. Thus, the term $r(x)$ represents an injection of mass at the point x_0 and an extraction of the same mass over the interval $[x_0, x_1]$.

Appendix B: Generic Solution Algorithm

[51] We outline here a generic solution algorithm based on approximating the 3-D distribution of salt mass fraction and water fluxes from the 2-D solution. In essence,

[52] Step 0: Initialization. Set the iteration counter i to 0 and solve flow for the sharp interface approximation to obtain ξ, the depth of the freshwater-saltwater interface. Actually, it is better to assume the interface a bit deeper. Here we used the approximation of *Pool and Carrera* [2011]:

$$\xi = -z_I = \sqrt{\frac{2Q_b x}{\epsilon^* K}}, \tag{B1}$$

where ϵ^* is the corrected density factor defined as $\epsilon^* = \epsilon\left[1 - (\alpha_T/b)^{1/6}\right]$. The initial salt mass fraction is defined as $\bar{\omega}^0 = [\omega_s(z_I - z_b)/(z_t - z_b)]$.

[53] Step 1: Given $\bar{\omega}^i$, $\bar{h}$ is computed solving the flow equation (13). Note that $\bar{h}$ is independent of $\bar{\omega}^i$ in constant thickness or horizontal bottom aquifers, such as in the Henry problem.

[54] Step 2: Estimate the width of the mixing zone (WMZ). Here we used the expression of *Abarca et al.* [2007a], WMZ $= 5.4\alpha_G$, where α_G is the geometric mean of the local dispersivity coefficients. The profile of $\omega(z)$ can then be obtained from $\bar{\omega}^i$, assuming a simplified form such as the one in the bottom of Figure B1 (dashed lines).

[55] Step 3: The freshwater head of the freshwater portion, h_f, and the saltwater head of the saltwater portion, h_s, are evaluated from $\bar{h}$ and z_I, Figure B1. Note that the width of the mixing zone and vertical fluxes are relevant for splitting $\bar{h}$ into its freshwater and saltwater portions. We have tested this split both assuming hydrostatic conditions ($\bar{q}_z = 0$) and $\bar{q}_z = \alpha_T \bar{q}_h/\mathrm{WMZ}$ (dispersive flux divided by ω_s). In our test, it can be neglected.

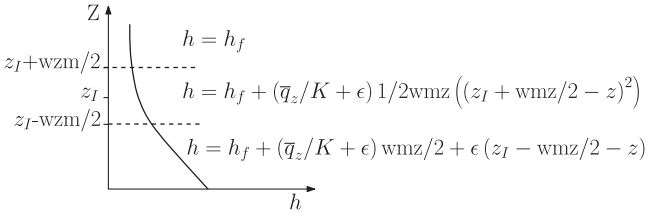

Figure B1. A vertical variation of head as a function of the width of the mixing zone and vertical fluxes.

[56] Step 4: Freshwater flux, q_f, and saltwater flux, q_s, are calculated using Darcy's law and h_f and h_s. Note that q_f and q_s must be such that the mean mass flux is equal to $\overline{\mathbf{u}}_h$, which was obtained in step 1. In 1-D, this implies

$$q_s \cong \frac{\overline{\mathbf{u}}_h}{\rho_s} \frac{z_t - z_b}{z_I - z_b} - \left[\frac{q_f}{1-\epsilon}\left(\frac{z_t - z_I}{z_I - z_b} + \frac{\epsilon}{2}\frac{\mathrm{WMZ}}{z_I - z_b}\right)\right]. \tag{B2}$$

This approximation allows more stable results than with Darcy's law and h_s in our examples (the difference was relatively small).

[57] Step 5: $\overline{\mathbf{u}_h\, \omega}$ is evaluated from q_f and q_s assuming the $\omega(z)$ profile of Figure 1 (bottom). The fluctuations about mean mass flux and salt mass fraction are calculated by $\overline{\mathbf{u}_h'\, \omega'} = \overline{\mathbf{u}_h\, \omega} - \overline{\mathbf{u}_h}\bar{\omega}$. Thus, equation (19) is solved to compute α_L^*.

[58] Step 6: Solve the transport equation (17) to get ω^{i+1}. In the 1-D examples presented in section 3.1, we have used finite differences, which yields

$$\bar{\omega}_j = \bar{\omega}_{j+1} \frac{(\alpha^*_{j+1/2} - \Delta x/2)}{(\alpha^*_{j+1/2} + \Delta x/2)}, \tag{B3}$$

where j is the cell number and the calculation starts at the shore, where the concentration is prescribed (recall section 2.4). When steps are present (case b in section 3.1), the cell is split in two, j^+ and j^-. Thus, ω_{j+} is computed using equation (B3); and ω_{j-}, which will be used for computing ω further inland, is obtained assuming the same elevation of the interface. That is,

$$\bar{\omega}_{j-} = [(z_{bj+} - z_{bj-} + \omega_{j+} + b_{j+}]/b_{j-}. \tag{B4}$$

[59] Step 7: The algorithm ends if $\omega^i \cong \omega^{i+1}$, that is, if the change in the solution between two consecutive iterations is negligible. Otherwise, the procedure sets $i = i + 1$ and returns to step 1.

[60] We had planned to correct WMZ (step 2) to ensure that the saltwater flux computed in step 4 is equal to the vertical dispersion flux mentioned in step 3. As it turned out, this correction was not needed in our examples, but may be needed in general.

[61] We have programmed this simple algorithm in a spreadsheet that can be download from http://www.h2ogeo.upc.es/software/RED/index.htm.

[62] **Acknowledgments.** The authors acknowledge the financial support provided by the European Commission (ATRAPO project, contract MEC CTM2007-66724-C02-01/TECNO) and the Spanish CICYT (HEROS project). M. Pool gratefully acknowledges an FI award from the Autonomous Government of Catalonia. We wish to thank Tissa Illangasekare for his comments on a preliminary versions of the manuscript. We also wish to thank A.E. and the reviewers for their constructive comments which significantly improved the quality of the manuscript.

References

Abarca, E. (2006), Seawater intrusion in complex geological environments, Ph.D. thesis, Technical University of Catalonia, Spain.

Abarca, E., E. Vazquez-Sune, J. Carrera, B. Capino, D. Gamez, and F. Batlle (2006), Optimal design of measures to correct seawater intrusion, *Water Resour. Res.*, *42*(9), W09415, doi:10.1029/2005WR004524.

Abarca, E., J. Carrera, X. Sanchez-Vila, and M. Dentz (2007a), Anisotropic dispersive henry problem, *Adv. Water Resour.*, *30*(4), 913–926.

Abarca, E., J. Carrera, X. Sanchez-Vila, and C. I. Voss (2007b), Quasi-horizontal circulation cells in 3D seawater intrusion, *J. Hydrol.*, *339*(3–4), 118–129.

Ataie-Ashtiani, B. (2007), Modsharp: Regional-scale numerical model for quantifying groundwater flux and contaminant discharge into the coastal zone, *Environ. Modell. Software*, *22*(9), 1307–1315.

Bakker, M. (1998), Transient dupuit interface flow with partially penetrating features, *Water Resour. Res.*, *34*(11), 2911–2918, doi:10.1029/98WR02366.

Bakker, M. (2003), A dupuit formulation for modeling seawater intrusion in regional aquifer systems, *Water Resour. Res.*, *39*(5), 1131, doi:10.1029/2002WR001710.

Bear, J. (1972), *Dynamics of Fluids in Porous Media*, 764 pp., Elsevier, Amsterdam, Netherlands.

Bear, J., A. H.-D. Cheng, V. Batu, C. Chen, X. Kuang, and J. Jimmy Jiao (2010), Methods to derive the differential equation of the free surface boundary, *Ground Water*, *48*, 486–493, doi:10.1111/j.1745-6584.2010.00711.x.

Bolster, D. T., D. M. Tartakovsky, and M. Dentz (2007), Analytical models of contaminant transport in coastal aquifers, *Adv. Water Resour.*, *30*(9), 1962–1972.

Chen, C., X. Kuang, and J. Jiao (2010), Methods to derive the differential equation of the free surface boundary, *Ground Water*, *48*(3), 329–332.

Cheng, A., D. Halhal, A. Naji, and D. Ouazar (2000), Pumping optimization in saltwater-intruded coastal aquifers, *Water Resour. Res.*, *36*(8), 2155–2165, doi:10.1029/2000WR900149.

Cooper, H. H., Jr. (1959), A hypothesis concerning the dynamic balance of fresh water and salt water in a coastal aquifer, *J. Geophys. Res.*, *64*(4), 461–467, doi:10.1029/JZ064i004p00461.

De Wiest, R. J. M., and J. Bear (1969), *Flow Through Porous Media*, 530 pp., Institute in Hydrology for College Teachers, Princeton University, Academic, N. Y.

Dentz, M., and J. Carrera (2005), Effective solute transport in temporally fluctuating flow through heterogeneous media, *Water Resour. Res.*, *40*(8), W08414, doi:10.1029/2004WR003571.

Dentz, M., and J. Carrera (2007), Mixing and spreading in stratified flow, *Phys. Fluid*, *19*(1), 17–107.

Dentz, M., D. M. Tartakovsky, E. Abarca, A. Guadagnini, X. Sanchez-Vila, and J. Carrera (2006), Variable-density flow in porous media, *J. Fluid. Mech.*, *561*, 209–235.

Frind, E. (1982), Simulation of long-term transient density-dependent transport in groundwater, *5*, 73–88.

Gasda, S. E., J. M. Nordbotten, and M. A. Celia (2009), Vertical equilibrium with sub-scale analytical methods for geological CO_2 sequestration, *Comput. Geosci.*, *13*(4), 469–481.

Gelhar, L. W., and C. L. Axness (1983), Three-dimensional stochastic analysis of macrodispersion in aquifers, *Water Resour. Res.*, *19*(1), 161–180, doi:10.1029/WR019i001p00161.

Gingerich, S., and C. Voss (2002), Three-dimensional variable-density flow simulation of a coastal aquifer in southern Oahu, Hawaii, USA, in *Proc SWIM17 Delft* 2002, edited by R. e. a. Boekelman, pp. 93–103, Delft Univ. Technology, Netherlands.

Held, R., S. Attinger, and W. Kinzelbach (2005), Homogenization and effective parameters for the Henry problem in heterogeneous formations, *Water Resour. Res.*, *41*, W11420, doi:10.1029/2004WR003674.

Henry, H. R. (1964), Effects of dispersion on salt encroachment in coastal aquifers, *Water-Supply Paper 1613-C*, pp. C71–84, *U.S. Geol. Surv.*

Hidalgo, J. J., L. J. Slooten, A. Medina, and J. Carrera (2005), *Groundwater And Saline Intrusion: Selected: Papers from the 18th Salt Water Intrusion Meeting, 18th SWIM, Cartagena* 2004, A Newton-Raphson based code for seawater intrusion modelling and parameter estimation, pp. 111–120, no. 15, Hidrogeología y Aguas Subterraneas, IGME, Madrid, Spain.

Hidalgo, J. J., J. Carrera, and M. Agustín (2009), Role of salt sources in density-dependent flow, *Water Resour. Res.*, *45*, W05503, doi:10.1029/2008WR007679.

Iribar, V., J. Carrera, E. Custodio, and A. Medina (1997), Inverse modelling of sea water intrusion in the Llobregat delta deep aquifer, *J. Hydrol.*, *198*(1–4), 226–244.

Kacimov, A. R., and M. M. Sherif (2006), Sharp interface, one-dimensional seawater intrusion into a confined aquifer with controlled pumping: Analytical solution, *Water Resour. Res.*, *42*(6), W06501, doi:10.1029/2005WR004551.

Lahm, T. D., E. S. Bair, and J. Vanderkwaak (1998), Role of salinity-derived variable-density flow in the displacement of brine from a shallow, regionally extensive aquifer, *J. Hydrol.*, *34*(6), 1469–1480.

Langevin, C. D. (2003), Simulation of submarine ground water discharge to a marine estuary: Biscayne Bay, Florida, *Ground Water*, *41*(6), 758–771.

Lin, J., J. B. Snodsmith, C. M. Zheng, and J. F. Wu (2009), A modeling study of seawater intrusion in Alabama gulf coast, USA, *Environ. Geol.*, *57*(1), 119–130.

Maas, C., and M. Emke (1988), Solving varying density groundwater problems with a single density computer program, *Natururwet. Tijdschr.*, *70*, 143–154.

Mantoglou, A. (2003), Pumping management of coastal aquifers using analytical models of saltwater intrusion, *Water Resour. Res.*, *39*(12), 1335, doi:10.1029/2002WR001891.

Mantoglou, A., M. Papantoniou, and P. Giannoulopoulos (2004), Management of coastal aquifers based on nonlinear optimization and evolutionary algorithms, *J. Hydrol.*, *297*(1–4), 209–228.

Nordbotten, J. M., and M. A. Celia (2006), An improved analytical solution for interface upconing around a well, *Water Resour. Res.*, *42*(8), W08433, doi:10.1029/2005WR004738.

Oude Essink, G. H. P. (2001a), Saltwater intrusion in 3D large scale aquifers: A Dutch case, *Phys. Chem. Earth* (*B*), *26*(4), 337–344.

Oude Essink, G. H. P. (2001b), Salt water intrusion in a three-dimensional groundwater system in the Netherlands: A numerical study, *Transp. Porous Media*, *43*(1), 137–158.

Oude Essink, G. H. P., and R. H. Boekelman (1996), Problems with large-scale modelling of salt water intrusion in 3D, *Proc. 14th Salt Water Intrusion Meeting*, Malmö, Sweden, pp. 16–31.

Paster, A., and G. Dagan (2007), Mixing at the interface between two fluids in porous media: A boundary-layer solution, *J. Fluid. Mech.*, *584*, 455–472.

Pinder, G. F., and M. A. Celia (2006), *Subsurface Hydrology*, 488 pp., John Wiley, Hoboken, N. J.

Pool, M., and J. Carrera (2011), A correction factor to account for mixing in Ghyben-Herzberg and critical pumping rate approximations of seawater intrusion in coastal aquifers, *Water Resour. Res.*, *47*, W05506, doi:10.1029/2010WR010256.

Qahman, K., and A. Larabi (2006), Evaluation and numerical modeling of seawater intrusion in the Gaza aquifer (Palestine), *Hydrogeol. J.*, *14*(5), 713–728.

Qahman, K., A. Larabi, D. Ouazar, A. Naji, and A. Cheng (2005), Optimal and sustainable extraction of groundwater in coastal aquifers, *Stoch. Env. Risk A.*, *19*(2), 99–110.

Sa da Costa, A. A. G., and J. L. Wilson (1979), A numerical model of seawater intrusion in aquifers, *Tech. Rep. 247*, Ralph M. Parsons Lab., MIT, Cambridge, Mass.

Sakr, S. A. (1999), Validity of a sharp-interface model in a confined coastal aquifer, *Hydrogeol. J.*, *7*(2), 155–160.

Simpson, M. J., and T. P. Clement (2003), Theoretical analysis of the worthiness of Henry and Elder problems as benchmarks of density-dependent groundwater flow models, *Adv. Water Resour.*, *26*, 17–31.

Smith, A. J. (2004), Mixed convection and density-dependent seawater circulation in coastal aquifers, *Water Resour. Res.*, *40*, W08309, doi:10.1029/2013WR002977.

Sorek, S., V. S. Borisov, and A. Yakirevich (2001), A two-dimensional areal model for density dependent flow regime, *Transp. Porous Media*, *43*(1), 87–105.

Strack, O. D. L. (1976), A single-potential solution for regional interface problems in coastal aquifers, *Water Resour. Res.*, *12*, 1165–1174, doi:10.1029/WR012i006p01165.

Vazquez-Sune, E., E. Abarca, J. Carrera, B. Capino, D. Gámez, M. Pool, T. Simó, F. Batlle, J. M. Niñerota, and X. Ibáñez (2006), Groundwater modelling as a tool for the European water framework directive (WFD) application: The llobregat case, *Phys. Chem. Earth*, *31*(17), 1015–1029.

Voss, C. I., and A. Provost (2002), SUTRA, a model for saturated-unsaturated variable-density ground-water flow with solute or energy transport, *Water Resources Investigations Report 02-4231, U.S. Geol. Surv.*

Voss, C. I., and W. R. Souza (1987), Variable density flow and transport simulation of regional aquifers containing a narrow freshwater-saltwater transition zone, *Water Resour. Res.*, *26*, 2097–2106, doi:10.1029/WR023i010p01851.

Weiss, E. (1982), A model for the simulation of flow of variable-density ground water in three dimensions under steady-state conditions, *U.S. Geol. Surv.*, 82–352.

Xue, Y., C. Xie, J. Wu, P. Lie, J. Wang, and Q. Jiang (1995), A 3-dimensional miscible transport model for seawater intrusion in China, *Water Resour. Res.*, *31*(4), 903–912, doi:10.1029/94WR02379.

Zhang, Q., R. E. Volker, and D. A. Lockington (2002), Experimental investigation of contaminant transport in coastal groundwater, *Adv. Environ. Res.*, *6*(3), 229–237.

E. Abarca and J. J. Hidalgo, Department of Civil and Environmental Engineering, Massachusetts Institute of Technology, 77 Massachusetts Ave., Cambridge, MA 20139-4307, USA.

J. Carrera and M. Dentz, Hydrogeology Group (GHS), Institute of Environmental Assessment and Water Research, CSIC, Jordi Girona 18, 08034 Barcelona, Spain.

M. Pool, Hydrogeology Group (GHS), Department of Geotechnical Engineering and Geosciences, Universitat Politecnica de Catalunya, UPC-BarcelonaTech, Jordi Girona 1-3, 08034 Barcelona, Spain. (maria.pool@idaea.csic.es)